Nanonization of Megestrol Acetate by Liquid Precipitation

ARTICLE *in* INDUSTRIAL & ENGINEERING CHEMISTRY RESEARCH · SEPTEMBER 2009

Impact Factor: 2.59 · DOI: 10.1021/ie900944y

6 AUTHORS, INCLUDING:

Jie-Xin Wang
Beijing University of Chemical Technology
57 PUBLICATIONS **1,235** CITATIONS
SEE PROFILE

Jimmy S. L. Yun
University of New South Wales
65 PUBLICATIONS **1,713** CITATIONS
SEE PROFILE

Nanonization of Megestrol Acetate by Liquid Precipitation

Zhi-Bing Zhang,[†] Zhi-Gang Shen,*[,†] Jie-Xin Wang,[†] Hong Zhao,[†] Jian-Feng Chen,*[,‡] and Jimmy Yun[§]

Sin-China Nano Technology Center, Key Lab for Nanomaterials, Ministry of Education, Beijing University of Chemical Technology, Beijing 100029, PR China, Research Center of the Ministry of Education for High Gravity Engineering and Technology, Beijing University of Chemical Technology, Beijing 100029, PR China, and Nanomaterials Technology Pte. Ltd., 28 Ayer Rajah Crescent no. 03-03, Singapore 139959, Singapore

The purpose of this study was to prepare megestrol acetate (MA) nanoparticles via a liquid precipitation technique. Several experimental parameters, such as the stabilizer combination, the volume ratio of antisolvent to drug solution, the temperature, the stirring speed, and the drying method were investigated. The as-prepared MA particles had a mean size of 208 nm, and 90% of the particles were distributed in the range of 100−300 nm, whereas the raw MA had a mean particle size of about 3.02 μm, ranging widely from 0.2 μm to 30 μm. X-ray diffraction (XRD), differential scanning calorimetry (DSC), and Fourier transform infrared (FTIR) analysis indicated that MA nanoparticles exhibited decreased crystallinity and unchanged chemical group structure after precipitation. The freeze-dried MA nanoparticles exhibited improved wettability as demonstrated by the contact angle measurement result proving that particles were covered by a hydrophilic layer. In dissolution rate tests, the nanoparticles achieved 100% drug dissolution within 5 min, while the raw MA did not dissolve completely after 120 min, suggesting that the dissolution property of MA nanoparticles was significantly enhanced.

1. Introduction

Megestrol acetate (MA), a biopharmaceutic class II drug with low solubility and high permeability,[1] is primarily used for the treatment of breast cancer and sometimes also prescribed to treat ovarian carcinoma and metastatic prostate carcinoma.[2−4] In recent years, MA has been increasingly described as an appetite stimulant for the treatment of cachexia related to AIDS and advanced cancer.[5,6] As a poorly water-soluble drug, MA features a low dissolution rate in the gastrointestinal tract, which limits its effective absorption and bioavailability.[7,8]

Nanoparticles are well known to improve the dissolution rate and bioavailability of poorly water-soluble drugs owing to increased surface area available for dissolution as described by the Noyes−Whitney equation.[9,10] Nanoparticles can be obtained either by reducing particle size of larger crystals (top-down approach) or by building up particles by precipitation of dissolved molecules (bottom-up approach).[11−15] Top-down techniques for drug nanocrystal production comprise media milling and high-pressure homogenization. Although commercially proven and widely used, these techniques are energy-intensive and time-consuming. Further, they have shown some disadvantages in practice such as the possible contamination with grinding media, inadequate control of particle size, and adverse effects of the high shear and temperature on the stability of the processed drugs. In the last decade, bottom-up techniques including supercritical fluid technology[16,17] and liquid precipitation[18−22] have been widely investigated to obtain nanoparticles. However, the supercritical fluid technique requires complex operating conditions and induces enormous production costs and, hence, is difficult to control and scale up.

In contrast, the liquid precipitation technique has good prospects because of its low cost, convenience in processing, and use of common equipment. The driving force of a precipitation process is the supersaturation of a solution created by mixing the drug solution and an antisolvent. The technique presents several advantages, in which it is a straightforward method, rapid and easy to perform. This technique has been successfully used to prepare nanosized hydrophobic drugs such as itraconazole,[18] cefuroxime axetil,[19] beclomethasone dipropionate,[21] and danazol.[22]

Nevertheless, the challenge in the liquid precipitation process is that most small-molecule drugs tend to form relatively large crystals within the range of 10−100 μm.[23] Moreover, for systems with water used as an antisolvent, the presence of hydrophobic particles or molecules after precipitation causes distortion and rearrangement of hydrogen bondings in the aqueous medium, therefore, greatly increasing the free energy of the system.[24] As a result, the primary particles in the slurry have a tendency to agglomerate. To hinder the growth and the agglomeration of particles, water-soluble polymers or/and charged surfactants have been used as stabilizers to modify the surface of the precipitated particles and lower the interfacial tension.[25,26] These two types of stabilizers are suspected to be adsorbed on the surface of particles acting as steric and electrostatic hindrances, respectively, so that particle agglomeration can be effectively prevented.[10,24]

To the best of our knowledge, no report is currently available on the preparation of MA nanoparticles by the liquid precipitation technique, and much attention has been paid to the nanomilling and supercritical fluid technology.[7,8] The objective of this study was to prepare MA nanoparticles by liquid precipitation in the presence of stabilizers. In addition, the experimental parameters were investigated, and the as-prepared MA nanoparticles were characterized by scanning electron microscopy (SEM), Fourier transform infrared spectroscopy

* To whom correspondence should be addressed. Tel.: +86-10-64447274. Fax: +86-10-64423474. E-mail address: shenzg@mail.buct.edu.cn (Z.G.S.). Tel.: +86-10-64446466. Fax: +86-10-64434784. E-mail address: chenjf@mail.buct.edu.cn (J.F.C.).

[†] Key Lab for Nanomaterials, Ministry of Education, Beijing University of Chemical Technology.

[‡] Research Center of the Ministry of Education for High Gravity Engineering and Technology, Beijing University of Chemical Technology.

[§] Nanomaterials Technology Pte. Ltd.

10.1021/ie900944y CCC: $40.75
Published on Web 08/20/2009

(FTIR), X-ray diffraction (XRD), differential scanning calorimetry (DSC), BET surface area analysis, contact angle measurement, and a dissolution rate test.

2. Experimental Section

2.1. Materials. Raw MA was supplied by Wuhan Yuancheng Technology Development Co., Ltd. (Hubei, China). Acetone (AR grade), sodium dodecyl sulfate (SDS), methylcellulose (MC), hydoxypropylmethylcellulose (HPMC), poloxamer 338 (F108), poloxamer 407 (F127), polyvinyl pyrrolidone (PVP K30), polyvinyl alcohol (PVA), and polyethylene glycol (PEG) were purchased from Chemical Reagent Company (Beijing, China). Deionized water was purified by Hitech-K Flow Water Purification System (Hitech instrument Co., Ltd. Shanghai, China).

2.2. Preparation of Nanosized Powder. Raw MA was firstly dissolved in acetone (20 mg/mL). The solution was then filtrated through a 0.45 μm nylon membrane to remove the possible particulate impurities to obtain clear MA solution. Afterwards, 10 mL of drug solution was quickly poured into the deionized water containing stabilizer(s) under magnetic stirring, and the precipitation occurred immediately. The precipitation process was performed in a thermostatic water bath to keep a constant temperature. After precipitation, the suspension was added dropwise to liquid nitrogen and freeze-dried using a model LT-105 lyophilizer (Martin Christ, Osterode, Germany) at a shelf temperature of −40°C and a pressure below 0.5 mbar for 48 h to yield dry powder. To evaluate the effects of drying methods, the suspension was also filtered, and the wet paste was dried in a normal oven at 60°C for 12 h.

2.3. Particle Size and Morphology. The morphology of MA samples was observed by scanning electron microscopy (SEM), JSM-6360LV (JEOL Inc., Japan). The dry powder or a glass slide with sample was fixed on an aluminum stub using double-sided adhesive tape and coated with gold. The column chart of the particle size distribution (PSD) was generated using the Image-Pro 5.1 (Media Cybernetics, Inc.) software according to the obtained SEM images. The width of the particle was prescribed as the specific particle size. Gauss fitting curves were also constructed to give an apparent illustration for PSD comparison.

2.4. Specific Surface Area. The specific surface area was measured using N_2 adsorption method. In this method, calculation was implemented by Surface Area Analyzer ASAP 2010-M (Micromeritics Instrument Corporation, USA) based on the BET equation. Before measuring, sample powder was degassed for at least 4 h.

2.5. Chemical Composition and Physical Characteristics. To eliminate the influence of stabilizers on chemical composition and physical characteristics of the processed MA, pure nanoparticles were specially prepared through filtration, repeated washing, and freeze-drying. FTIR analysis was carried out to evaluate the molecular states of raw MA and MA nanoparticles. FTIR spectra were recorded with a Nicolet model 8700 spectrometer (Nicolet thermo electron instrument corporation, USA) in the range of 400−4000 cm^{-1} using a resolution of 2 cm^{-1} and 32 scans. Samples were diluted with 1% of KBr mixing powder and pressed to obtain self-supporting disks.

X-ray diffraction (XRD) was employed to detect any changes in physical characteristics and the crystallinity of MA nanoparticles using a XRD-6000 diffractometer (Shimadzu Inc., Japan). The sample powder was placed in an aluminum sample holder. Cu $K_{\alpha 1}$ radiation was generated at 30 mA and 40 kV. The scanning speed was 5°/min from 5° to 50° with a step size of 0.05°.

The thermal behaviors of samples were analyzed by a differential scanning calorimeter (Q200, TA, USA) at a heating rate of 10°C /min. A dry nitrogen purge of 20 mL/min was employed in the process. Calibration of the instrument with respect to temperature and enthalpy was achieved using a high purity standard of indium.

2.6. Contact Angle Measurement. The contact angle was measured by the sessile drop technique using a goniometer (OCA20, Dataphysics, Germany). Compressed discs of the powders were made at a 30 MPa compression force using a laboratory powder press (model 769YP-15A, Tianjin, China). A droplet of purified water was placed onto the surface of the compressed disc and observed through a low-power microscope. The contact angle was determined by measuring the tangent of the droplet on the disc surface.

2.7. Dissolution Rate Test. Dissolution tests were carried out using a dissolution apparatus (D-800LS, Tianjin, China) following the USP Apparatus II (paddle) method. The paddle speed and bath temperature were set at 100 rpm and 37.0 ± 0.5 °C, respectively. A 1% SDS aqueous solution was employed as the dissolution medium. The dissolution rate tests were performed at sink conditions. A 100 mg sample of raw MA or nanosized MA powder was respectively added into different vessels containing 900 mL dissolution medium. A 5 mL aliquot was taken each time at specific time intervals and immediately filtered through a 0.10 μm syringe filter. In the meantime, fresh medium (5 mL) was added to keep a constant volume. The filtrate was appropriately diluted, and the drug concentration was calculated based on the absorbance value read by a UV spectrophotometer (UV-2501, Shimadzu, Japan) at 292 nm. The dissolution test of each sample was performed in triplicate.

3. Results and Discussion

3.1. Selection of Stabilizers. Preparation of drug nanoparticles usually requires a careful selection of stabilizers. In our experiment, eight stabilizers including seven different polymers (e.g. HPMC, MC, PEG, F108, F127, PVP K30, and PVA) and a charged surfactant (e.g. SDS) were evaluated. The concentration of each stabilizer solution was 0.02%. It was found that particles agglomerated heavily when only one stabilizer was employed. Often, effective stabilization can be achieved through the combined use of a polymer and a charged surfactant;[14,27] therefore, the above-mentioned polymers were tested together with SDS, respectively. Both concentrations of stabilizers in deionized water were set at 0.02%. However, among all combinations investigated, only PVP and SDS could help to form a well-dispersed nanosuspension with a mean particle size less than 400 nm. In addition, it was worth noting that, at a constant PVP/drug weight ratio of 1/10, the mean size and morphology of the precipitated particles changed slightly with the decrease of SDS concentration from 0.02% to 0.002%. Figure 1 shows SEM images of raw MA and processed MA particles using different stabilizer combinations. The raw MA had an irregular morphology and a mean particle size of ∼3.02 μm with a wide particle size distribution (PSD) from 0.2 to 30 μm (Figure 1A). The nanoparticles precipitated in the presence of PVP and SDS appeared rod-like within the 100−1000 nm size range (Figure 1B). In comparison, irregular flake-shaped particles in the range of 300−3000 nm were precipitated in the presence of PEG and SDS (Figure 1C).

The efficiency of the combination of PVP and SDS might be explained by the sufficient surface coverage of a PVP/SDS complex layer on the particle surface resulting in the stabilizing effects.[27] On the contrary, insufficient surface coverage of stabilizers on the particles would induce rapid agglomeration of primary particles in the case of any other stabilizer combination. Thus, the combination of PVP and SDS could be a potential candidate for drug nanoparticle formation and stabilization in the liquid precipitation process.

3.2. Effect of AS/S Volume Ratio. The particle morphology and the PSD obtained at various volume ratios of antisolvent to drug solution (AS/S) are reported in Figure 2A−E. It was obvious that the particles obtained at different volume ratios exhibited the similar rodlike morphology. With the increase of the AS/S ratio from 5 to 10, the mean size decreased notably. However, when the AS/S volume ratio increased further, only slight change in the mean size and the PSD was observed. The shift from a larger particle size at lower volume ratio to a smaller particle size at higher volume ratio can be explained as follows.

Precipitation mainly includes two steps: nucleation and crystal growth. The driving force of nucleation is supersaturation ratio (S) which is given by eq 1[28]

$$S = \frac{C}{C^*} \tag{1}$$

where C and C^* are the MA concentration in acetone and the saturation concentration of MA in the acetone−water mixture, respectively. When the AS/S ratio increased, the supersaturation level increased due to the decrease of saturation concentration. As shown in Figure 2F, the solubility decreased greatly before a value of 8 for the AS/S ratio and, then, slowly decreased before a value of 25 for the AS/S ratio. According to the classical nucleation theory, a higher level of supersaturation would lead to a faster nucleation rate and a smaller critical nucleus size. Therefore, the number of homogenously formed nuclei increased with the increase of the AS/S ratio. On the other hand, the crystal growth rate can be expressed as[29,30]

$$\frac{dl}{dt} = K_g(C_i - C^*)^b \tag{2}$$

where K_g is the crystal growth rate constant; C_i and C^* are the solute concentration on the crystal surface and saturation concentration, respectively. The value of the parameter b is usually between 1 and 3 and decreases with a reduction of temperature. The increased antisolvent volume virtually decreased the solute concentration on the formed MA crystal surface. Therefore, the decreased value of $C_i - C^*$ resulted in a slower crystal growth rate, thereby resulting in a smaller ultimate particle size. However, when the AS/S volume ratio was higher than 10, the value of $C_i - C^*$ had already achieved a relatively constant level, leading to no obvious further decrease in particle size.

3.3. Effect of Temperature. Figure 3A and B reveals that temperature has a significant effect on the particle size and morphology. It was evident that the precipitated particles had an irregular flakelike morphology with a mean size of about 2 μm at 30 °C; while the particles presented rodlike morphology with size around 240 nm obtained at 3 °C. This indicated that the lower the precipitation temperature, the smaller the particles. The following reasons may be responsible for this phenomenon. First, the solubility of MA in the acetone−water mixture decreased; therefore, increasing the level of supersaturation upon mixing, as shown in Figure 3C. Lower solubility also decreased the rate of Ostwald ripening. Second, the precipitation in the liquid phase is a diffusion-limited process.[31] Low temperature would decrease the diffusion and growth kinetics at the crystal boundary layer interface, which was confirmed by eq 2. As a result, lower temperatures led to smaller particles.

3.4. Effect of Stirring Speed. Figure 4 shows SEM images and the corresponding PSD of MA particles precipitated under different stirring speeds. The mean particle size decreased from 263 to 208 nm with a stirring speed increasing from 500 to 2500 rpm. Moreover, with the increase in stirring speed, the PSD became narrower and 90% of the particles prepared at 2500

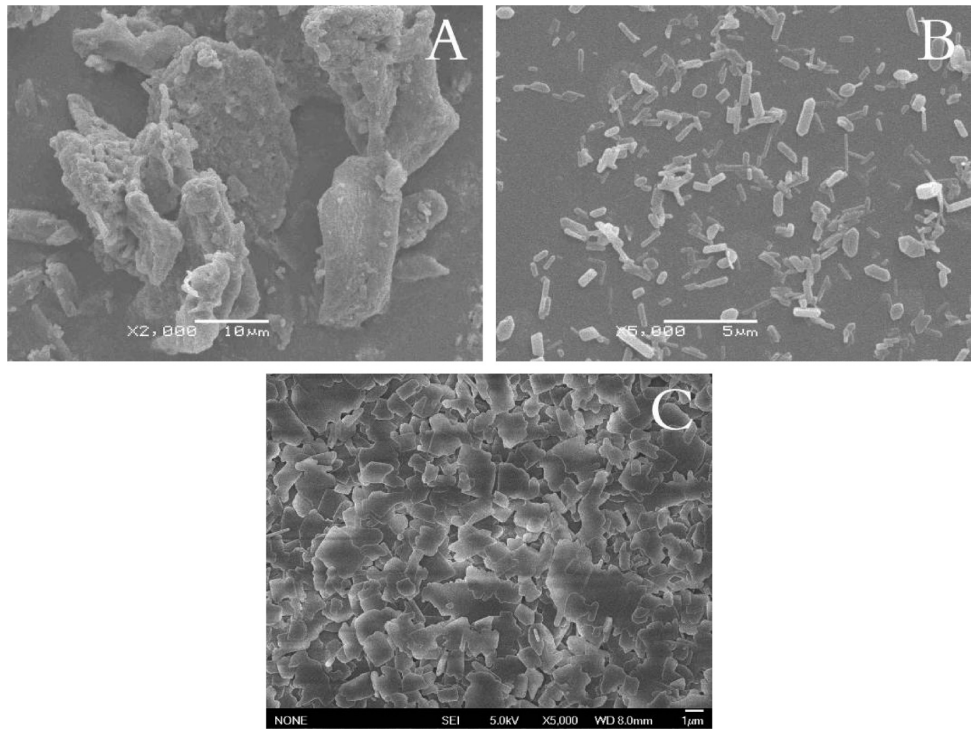

Figure 1. SEM images of (A) raw MA, (B) nanoparticles precipitated in the presence of PVP and SDS, and (C) particles precipitated in the presence of PEG and SDS.

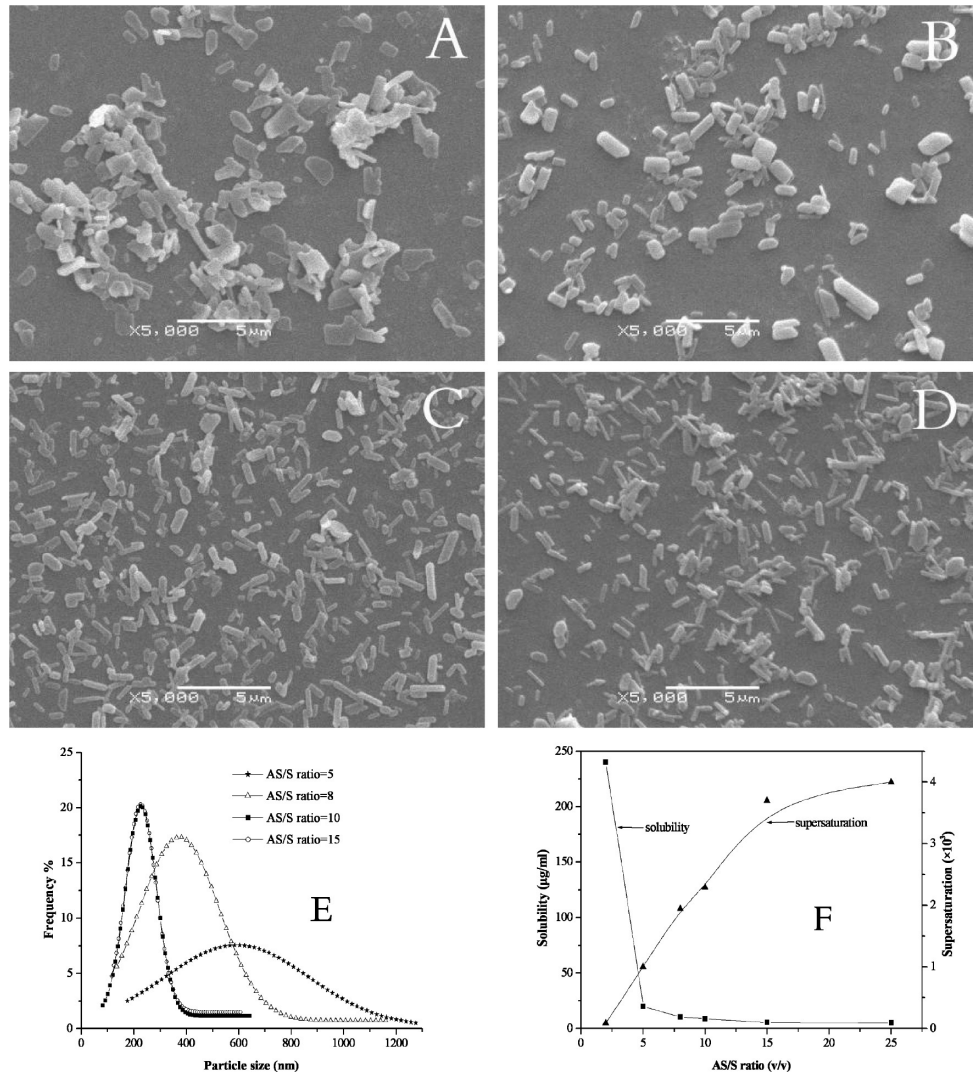

Figure 2. SEM images of MA particles prepared at different AS/S ratios: (A) AS/S = 5; (B) AS/S = 8; (C) AS/S = 10; (D) AS/S = 15. (E) Particle size distributions of MA particles prepared at different ratios. (F) Effect of AS/S volume ratio on the terminal solubility of MA in acetone−water mixture and the terminal value of *S*.

rpm were distributed in the range of 100−300 nm. The mechanism of the particle size decrease can be explained by the intensification of the micromixing (i.e. mixing on the molecular level) between different phases with the increase in stirring speed. High micromixing efficiency enhanced the mass transfer and the rate of diffusion between phases, which induced great supersaturation in a short time and subsequent rapid nucleation to generate smaller particles in a narrower size distribution.[18] Therefore, high stirring speed favored the formation of small particles with a narrow PSD.

3.5. Effect of Drying Methods. Freeze-drying, a process which consists of removing water from a frozen sample by sublimation and desorption under vacuum, is one of the most commonly used methods to convert solutions or suspensions into solids of sufficient stability for distribution and storage in the pharmaceutical field.[32,33] When an MA nanosuspension was freeze-dried, the obtained powder was incompact and, more importantly, the particles could be redispersed uniformly in deionized water with nearly no change in particle size and morphology, as shown in Figure 5A. Comparatively, if the nanosuspension was filtered and dried in an oven, the particles aggregated heavily and could not be completely pulverized, even though the size and morphology of the primary particles were similar to those particles in suspension prior to drying (Figure 5B).

3.6. FTIR, XRD, and DSC Analysis. FTIR analysis was performed to evaluate the molecular status of raw MA and processed MA nanoparticles. The corresponding FTIR spectra are presented in Figure 6. The identical FTIR spectra curves suggested that the addition of stabilizers and the employment of the liquid precipitation process did not affect the chemical composition of MA.

The XRD patterns of raw MA and MA nanoparticles are displayed in Figure 7. Obviously, two samples had almost the same peak positions, indicating that the liquid precipitation process had no effect on the physical characteristics of MA. It could also be seen that the peaks of MA nanoparticles exhibited lower intensities than those of raw MA suggesting lower crystallinity and smaller particle size of the MA nanoparticles.

To further confirm the physical state, DSC was performed to analyze the raw MA and MA nanoparticles. The results DSC studies are given in Figure 8. The raw MA showed a sharp endotherm at 211.3 °C (with an enthalpy of 110.0 J/g) corresponding to its melting point. In comparison, the nanoparticles had an endotherm at 206.1 °C (with an enthalpy of

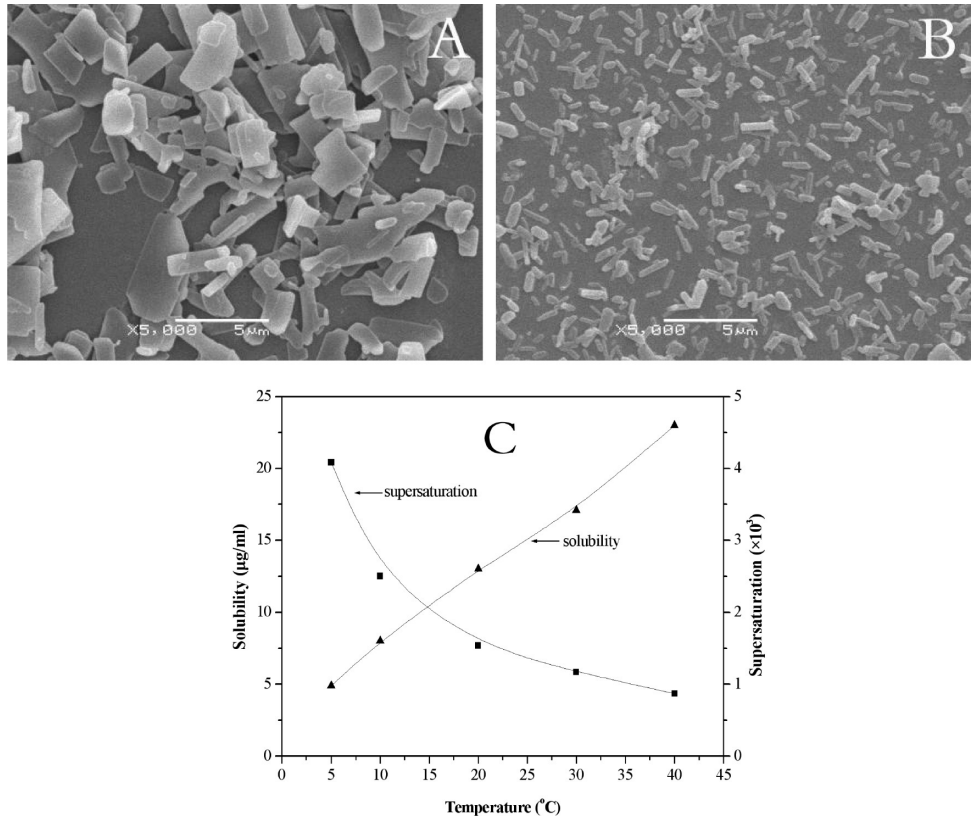

Figure 3. SEM images of MA particles prepared at (A) 30 and (B) 3 °C. (C) Effect of temperature on the terminal solubility of MA in an acetone−water mixture and the terminal value of *S*.

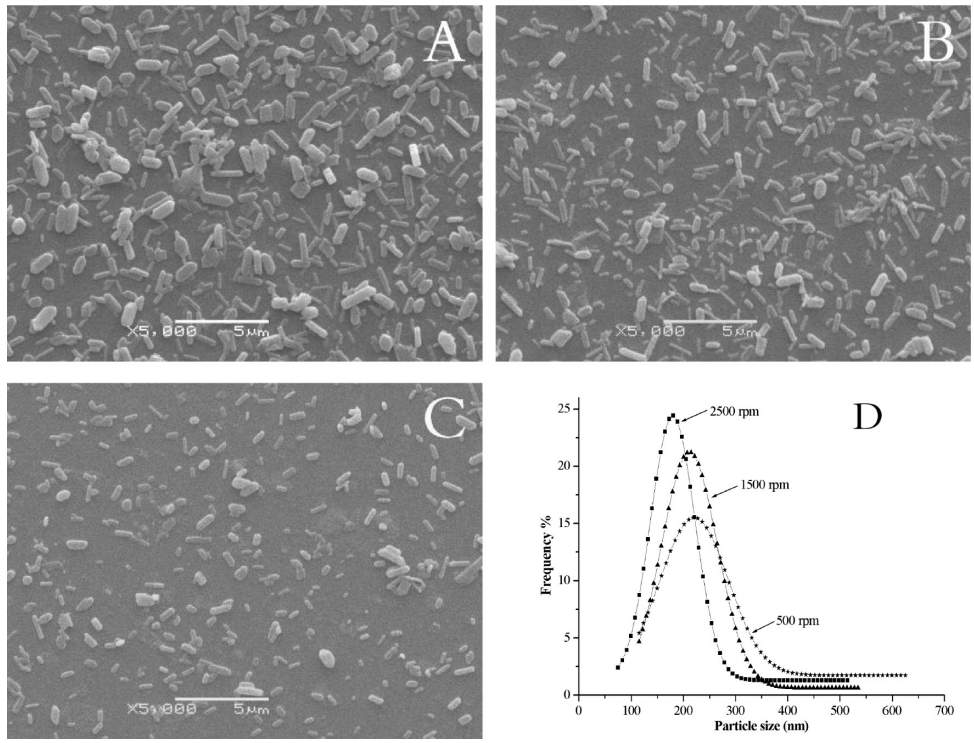

Figure 4. SEM images of MA particles prepared under (A) 500, (B) 1500, and (C) 2500 rpm. (D) Particle size distributions of MA particles prepared under different stirring speeds.

95.7 J/g). This reduction in melting point and enthalpy could be attributed to the decreased crystallinity, which agreed with the XRD analysis. It is believed that poorly water-soluble drugs with lower crystallinity and smaller size usually exhibit faster dissolution rate and better bioavailability.[34] Therefore, the processed MA nanoparticles are expected to have faster dissolution rate and better bioavailability as compared to the raw MA particles.

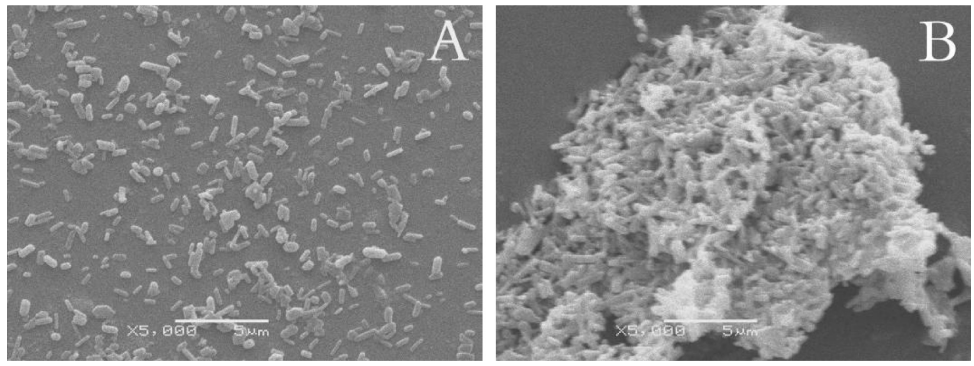

Figure 5. SEM images of (A) redispersed freeze-dried particles and (B) oven dried particles.

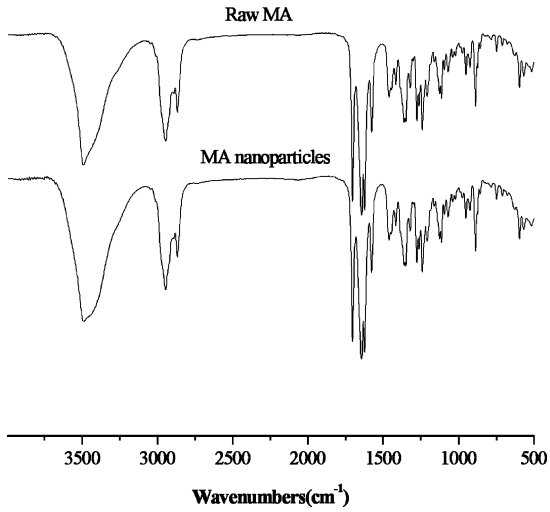

Figure 6. FTIR spectra of raw MA and nanoparticles.

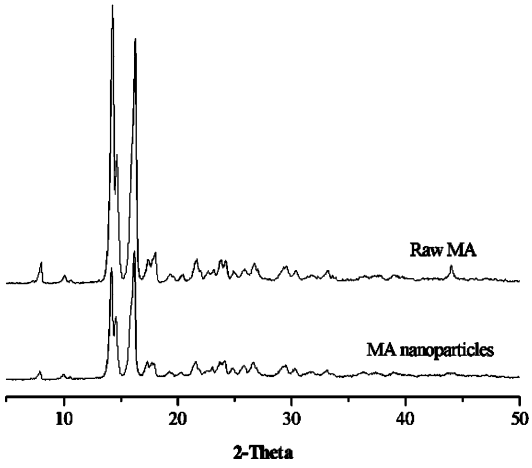

Figure 7. XRD patterns of raw MA and nanoparticles.

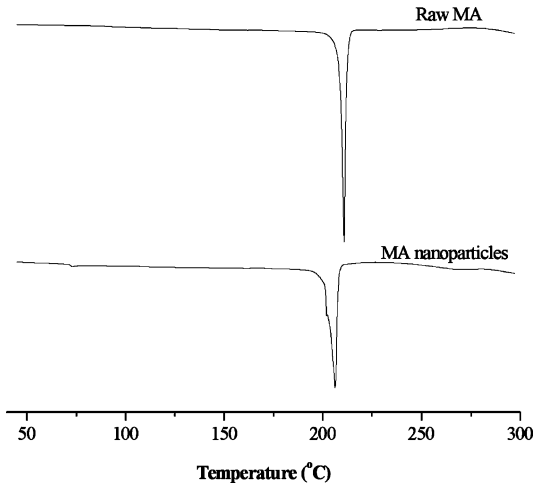

Figure 8. DSC curves of raw MA and nanoparticles.

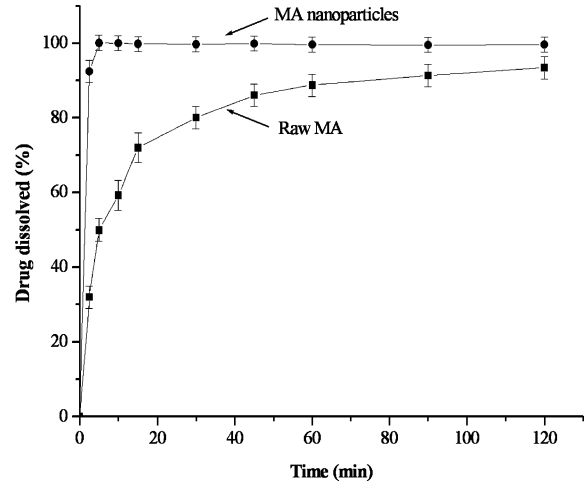

Figure 9. Dissolution rate tests for raw MA and MA nanoparticles.

3.7. Wettability. The wettability of raw MA and nanosized MA was evaluated by measuring the contact angle at the purified water/compacted powder interface. Under optimum conditions, the weight ratio of MA/PVP/SDS in suspension was 1/0.1/0.01, and the drug loading of the freeze-dried powder was about 90%. The contact angle was evidently decreased from ~61° for the raw drug to ~31° for the nanosized drug, indicating that the surface of MA nanoparticles was hydrophilized due to the adsorbed hydrophilic stabilizers. Thus, by precipitating nanoparticles in the presence of stabilizers, a large and hydrophilized surface can be formed in a one-step process without using any milling techniques.

3.8. Dissolution Rate Test. The dissolution profiles of raw MA and nanosized MA were compared, and the results are presented in Figure 9. MA nanoparticles reached 100% drug dissolution within 5 min. However, only 49% of raw MA was dissolved during the same period. Furthermore, the raw MA achieved an incomplete dissolution (~93%) after 120 min. The results revealed that the dissolution property of MA after nanonization was significantly enhanced. The enhancement in dissolution rate could be attributed to the reduced particle size (from 3.02 to 208 nm), the enlarged BET surface area (from 3.93 to 15.97 m^2/g), and the decreased contact angle (from 61° to 31°).

4. Conclusion

In this study, MA nanoparticles were prepared using liquid precipitation technique with PVP and SDS as stabilizers. The effects of various AS/S volume ratios, precipitation temperatures, and stirring speeds on the mean particle size and size distribution of MA were investigated. With the increase in AS/S ratio and stirring speed and the decrease in precipitation temperature, the particle size exhibited a decreasing tendency. Under optimum conditions, MA nanoparticles with a mean size of 208 nm were successfully prepared, and 90% of the particles were distributed in the range of 100−300 nm. Compared to the raw MA, the precipitated nanoparticles showed decreased crystallinity and very similar chemical composition. More importantly, the dissolution rate of MA nanoparticles within 5 min was enhanced from 49% to 100% owing to a decreased particle size from 3.02 μm to 208 nm, an enlarged specific surface area from 3.93 to 15.97 m^2/g, and a decreased contact angle from about 61° to 31°. Therefore, liquid precipitation would offer a great opportunity for poorly water-soluble drugs to achieve nanosized particles with a rapid dissolution rate.

Acknowledgment

This work was financially supported by National Natural Science Foundation of China (Nos. 20806004 and 20821004) and the Talent Training Program of Beijing City (2007B022).

Literature Cited

(1) Deng, Z. Y.; Zhao, R. P.; Dong, L. C.; Wong, G. Characterization of nanoparticles for drug delivery applications. *Microsc. Microanal.* **2005**, *11*, 1934–1935.

(2) Gregory, E. J.; Cohen, S. C.; Oines, D. W.; Mims, C. H. Megestrol acetate therapy for advanced breast cancer. *J. Clin. Oncol.* **1985**, *3*, 155–160.

(3) Sikic, B. I.; Scudder, S. A.; Ballon, S. C.; Soriero, O. M.; Christman, J. E.; Suey, L.; Ehsan, M. N.; Brandt, A. E.; Evans, T. L. High dose megestrol acetate therapy of ovarian carcinoma: a phase II study by the Northern California Oncology Group. *Semin. Oncol.* **1986**, *13*, 26–32.

(4) Johnson, D. E.; Babaian, R. J.; Swanson, D. A.; Von Eschbach, A. C.; Wishnow, K.; Tenney, D. Medical castration using megestrol acetate and mini dose estrogens. *Urology.* **1988**, *31*, 371–374.

(5) Aisner, J.; Parnes, H.; Tait, N.; Hickmam, M.; Forrest, A.; Greco, F. A.; Tchekmedyian, N. S. Appetite stimulation and weight gain with megestrol acetate. *Semin. Oncol.* **1990**, *17*, 2–7.

(6) Strang, P. The effect of megestrol acetate on anorexia, weight loss and cachaexia in cancer and AIDS patients. *Anticancer Res.* **1997**, *17*, 657–662.

(7) Shekunov, B. Y.; Chattopadhyay, P.; Seitzinger, J.; Huff, R. Nanoparticles of poorly water-soluble drugs prepared by supercritical fluid extraction of emulsions. *Pharm. Res.* **2006**, *23*, 196–204.

(8) Hovey, D.; Pruitt, J.; Ryde, T. *Nanoparticulate megestrol formulations*. U.S. Patent 20050008707, 2005.

(9) Patravale, V. B.; Date, A. A.; Kulkarni, R. M. Nanosuspensions: a promising drug delivery strategy. *J. Pharm. Pharmacol.* **2004**, *56*, 827–840.

(10) Kesisoglou, F.; Panmai, S.; Wu, Y. Nanosizing—oral formulation development and biopharmaceutical evaluation. *Adv. Drug Delivery Rev.* **2007**, *5916*, 31–44.

(11) Van Eerdenbrugh, B.; Van den Mooter, G.; Augustijns, P. Top-down production of drug nanocrystals: Nanosuspension stabilization, miniaturization and transformation into solid products. *Int. J. Pharm.* **2008**, *364*, 64–75.

(12) Rogers, T. L.; Nelsen, A. C.; Hu, J. H.; Brown, J. N.; Sarkari, M.; Young, T. J.; Johnston, K. P.; Williams, R. O., III. A novel particle engineering technology to enhance dissolution of poorly water-soluble drugs: spray-freezing into liquid. *Eur. J. Pharm. Biopharm.* **2002**, *54*, 271–280.

(13) Hu, J. H.; Johnston, K. P.; Williams, R. O., III. Rapid dissolving high potency danazol powders produced by spray freezing into liquid process. *Int. J. Pharm.* **2004**, *271*, 145–154.

(14) Merisko-Liversidge, E.; Liversidge, G. G.; Cooper, E. R. Nanosizing: a formulation approach for poorly-water-soluble compounds. *Eur. J. Pharm. Sci.* **2003**, *18*, 113–120.

(15) Jacobs, C.; Kayser, O.; Müller, R. H. Nanosuspensions as a new approach for the formulation for the poorly soluble drug tarazepide. *Int. J. Pharm.* **2000**, *196*, 161–164.

(16) Tandya, A.; Dehghani, F.; Foster, N. R. Micronization of cyclosporine using dense gas techniques. *J. Supercrit. Fluids* **2006**, *37*, 272–278.

(17) Chattopadhyay, P.; Gupta, R. B. Production of griseofulvin nanoparticles using supercritical CO_2 antisolvent with enhanced mass transfer. *Int. J. Pharm.* **2001**, *228*, 19–31.

(18) Matteucci, M. E.; Hotze, M. A.; Johnston, K. P.; Williams, R. O., III. Drug nanoparticles by antisolvent precipitation: mixing energy versus surfactant stabilization. *Langmuir* **2006**, *22*, 8951–8959.

(19) Zhang, J. Y.; Shen, Z. G.; Zhong, J.; Hu, T. T.; Chen, J. F.; Ma, Z. Q.; Yun, J. Preparation of amorphous cefuroxime axetil nanoparticles by controlled nanoprecipitation method without surfactants. *Int. J. Pharm.* **2006**, *323*, 153–160.

(20) Park, S. J.; Jeon, S. Y.; Yeo, S. D. Recrystallization of a pharmaceutical compound using liquid and supercritical antisolvents. *Ind. Eng. Chem. Res.* **2006**, *45*, 2287–2293.

(21) Wang, Z.; Chen, J. F.; Le, Y.; Shen, Z. G.; Yun, J. Preparation of ultrafine beclomethasone dipropionate drug powder by antisolvent precipitation. *Ind. Eng. Chem. Res.* **2007**, *46*, 4839–4845.

(22) Zhao, H.; Wang, J. X.; Wang, Q. A.; Chen, J. F.; Yun, J. Controlled liquid antisolvent precipitation of hydrophobic pharmaceutical nanoparticles in a microchannel reactor. *Ind. Eng. Chem. Res.* **2007**, *46*, 8229–8235.

(23) Kashchiev, D. *Nucleation: Basic Theory with Applications*; Butterworth-Heinemann: Oxford, 2000.

(24) Ain-Ai, A.; Gupta, P. K. Effect of arginine hydrochloride and hydroxypropyl cellulose as stabilizers on the physical stability of high drug loading nanosuspensions of a poorly soluble compound. *Int. J. Pharm* **2008**, *351*, 282–288.

(25) Rasenack, N.; Steckel, H.; Müller, B. W. Preparation of microcrystals by in situ micronization. *Powder Technol.* **2004**, *143−144*, 291–296.

(26) Pozarnsky, G. A.; Matijević, E. Preparation of monodisperse colloids of biologically active compounds 1. Naproxen. *Colloids Surf. A: Physicochem. Eng. Aspects* **1997**, *125*, 47–52.

(27) Pongpeerapat, A.; Wanawongthai, C.; Tozuka, Y.; Moribe, K.; Yamamoto, K. Formation mechanism of colloidal nanoparticles obtained from probucol/PVP/SDS ternary ground mixture. *Int. J. Pharm* **2008**, *352*, 309–316.

(28) Dirksen, J. A.; Ring, T. A. Fundamentals of crystallization: kinetic effects on particles size distributions and morphology. *Chem. Eng. Sci.* **1991**, *46*, 2389–2427.

(29) Horn, D.; Rieger, J. Organic nanoparticles in the aqueous phase—theory, experiment, and use. *Angew. Chem. Int. Ed.* **2001**, *40*, 4330–4361.

(30) Chen, J. F.; Zhou, M. Y.; Shao, L.; Wang, Y. Y.; Yun, J.; Chew, N. Y. K.; Chan, H. K. Feasibility of preparing nanodrugs by high-gravity reactive precipitation. *Int. J. Pharm.* **2004**, *269*, 267–274.

(31) Nielsen, A. E. *Kinetics of Precipitation*; Pergamon Press: Oxford, 1964.

(32) Abdelwahed, W.; Degobert, G.; Stainmesse, S.; Fessi, H. Freeze-drying of nanoparticles: Formulation, process and storage considerations. *Adv. Drug Delivery Rev.* **2006**, *58*, 1688–1713.

(33) Matteucci, M. E.; Paguio, J. C.; Miller, M. A.; Williams, R. O., III; Johnston, K. P. Flocculated amorphous nanoparticles for highly supersaturated solutions. *Pharm. Res.* **2008**, *25*, 2477–2487.

(34) Sarkari, M.; Brown, J.; Chen, X. X.; Swinnea, S.; Williams, R. O., III; Johnston, K. P. Enhanced drug dissolution using evaporative precipitation into aqueous solution. *Int. J. Pharm.* **2002**, *243*, 17–31.

Received for review June 9, 2009
Revised manuscript received July 23, 2009
Accepted August 6, 2009

IE900944Y